Characterization of acetyl-CoA synthetase kinetics and ATP-binding

Julia Gallego-Jara[1]*, Gema Lozano Terol[1]*, Ana Écija Conesa[1], Barbara Zambelli[2], Manuel Cánovas Díaz[1] and Teresa de Diego Puente[1].

[1]Department of Biochemistry and Molecular Biology and Immunology (B), Faculty of Chemistry, University of Murcia, Campus of Espinardo, Regional Campus of International Excellence ‘‘Campus Mare Nostrum’’, P.O. Box 4021, Murcia E-30100, Spain.

[2]Laboratory of Bioinorganic Chemistry, Department of Pharmacy and Biotechnology, University of Bologna, Via Giuseppe Fanin 40, I-40127 Bologna, Italy.

*Corresponding author

Email: julia.gallego@um.es and gema.lozano@um.es; Tel.: +34868887397; Fax: +34968364148.

Abstract

Background

The superfamily of adenylating enzymes is a large family of enzymes broadly distributed from bacteria to humans. Acetyl-CoA synthetase (Acs), member of this family, is a metabolic enzyme with an essential role in *Escherichia coli* (*E. coli*) acetate metabolism, whose catalytic activity is regulated by acetylation/deacetylation *in vivo*.

Methods

In this study, the kinetics and thermodynamic parameters of deacetylated and acetylated *E. coli* Acs were studied for the adenylating step. Moreover, the role of the T264, K270, D500 and K609 residues in catalysis and ATP-binding was also determined by Isothermal titration calorimetry.

Results

The results showed that native Acs enzyme binds ATP in an endothermic way. The dissociation constant has been determined and ATP-binding showed no significant differences between acetylated and deacetylated enzyme, although k_{cat} was much higher for the deacetylated enzyme. However, K609 lysine mutation resulted in an increase in ATP-Acs-affinity and in a total loss of enzymatic activity, while T264 and D500 mutant proteins showed a total loss of ATP-binding ability and a decrease in catalytic activity. K609 site-specified acetylation induced a change in Acs conformation which resulted in an exothermic and more energetic ATP-binding.

Conclusions

The differences in ATP-binding could explain the broadly conserved inactivation of Acs when K609 is acetylated.

General Significance

The results presented in this study demonstrate the importance of the selected residues in Acs ATP-binding and represent an advance in our understanding of the adenylation step of the superfamily of adenylating enzymes and of their acetylation/deacetylation regulation.

Keywords: *Escherichia coli*; Acetyl-CoA synthetase; ITC; ATP; lysine acetylation.

1. Introduction

The ANL superfamily of adenylating enzymes contains acyl- and aryl-CoA synthetases, firefly luciferase, and the adenylation domains of the modular non-

ribosomal peptide synthetases (NRPSs). ANL enzymes are broadly distributed in prokaryotes and eukaryotes and share a sequence identity of ~20 %. Although ANL enzymes show differences in their respective catalytic mechanisms, all of them are structurally homologous and share a global mechanism of two-step catalysis: a first adenylation reaction and a diverse set of second partial reactions [1]. Accordingly, acyl- and aryl-CoA synthetases catalyse the activation of a wide variety of carboxylates into the acyl- aryl-CoA derivatives in two independent reactions, as was described in 1956 by Paul Berg [2]. In the first step the carboxylate is activated into a carboxyl-AMP intermediate. Subsequently, a CoASH molecule reacts with the adenylate intermediate to lead to the acyl- aryl-CoA and AMP. Carboxylic substrates can vary from acetate (2C) to long fatty acids such as myristic acid (14C). Acyl-CoA formation has been widely studied for 60 years [2] and a ping-pong kinetic mechanism has been established for many of these synthetases [3–7] (Figure 1A).

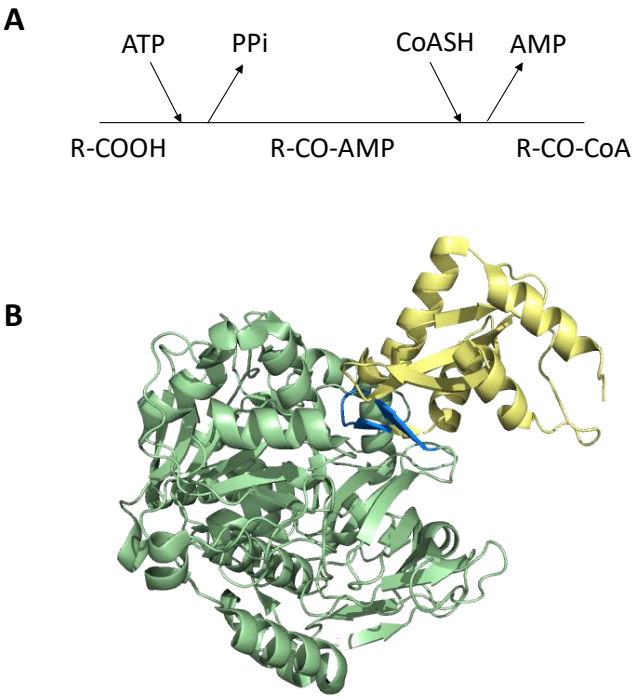

Figure 1. (A) Acyl- and aryl-CoA synthetases ping-pong mechanism. **(B)** Crystallographic structure of *Salmonella enterica* acetyl-CoA synthetase (PDB ID: 1PG4). The N- domain is colored in green, C-terminal domain is colored in yellow and A8 loop is shown in blue.

The structure of the ANL superfamily of adenylating enzymes is formed by a long non-catalytic N-terminal domain and a short C-terminal domain containing the main catalytic residues (Figure 1B). The substrates are positioned at the interface of the two

domains. All ANL enzymes are flexible proteins, and were found in two different conformations that differ for the position of the C-terminal domain that rotates of ~ 140 º [1]: an adenylating or closed conformation carries out the first catalytic reaction, while a second open conformation (called thioester-forming conformation for acyl-CoA synthases) is responsible for the final catalytic step. Proteins belonging from the ANL superfamily contain ten highly conserved motifs (A1-A10). Several conserved residues have been shown to be involved in ATP-binding in the structures crystalized in the presence of ATP [8–16]: an aspartic acid (D500 in *E. coli* Acs) from A7 domain interacts through hydrogen bonds with the ATP ribose molecule [9,11,14,16], an arginine (R519 in *E. coli* Acs) from A8 domain binds the β-phosphate of the PPi [8–11,14], a lysine (K609 in *E. coli* Acs) from A10 domain coordinates ATP pyrophosphate, together with a conserved phosphate binding loop (P-loop) (S/T)(S/T/G)G(S/T)TGxPK (residues 264-272 in *E. coli* Acs) from A3 domain, which binds the beta and gamma phosphates of pyrophosphate [8–13,15,16].

Acetyl-CoA synthetase is an important metabolic enzyme for prokaryote and eukaryote organisms. Its physiological role is to activate acetate to acetyl-CoA to be used in several metabolic routes. Prokaryotic organisms, such as *E. coli*, can consume acetate from the environment as carbon source, converting it to acetyl-CoA by two independent routes, one catalysed by Acs [17,18]. The enzyme, as other AMP-forming synthetases, is regulated by reversible acetylation of the conserved lysine in A10 domain (K609 in *E. coli* Acs) [19–24]. Acetylation inhibits the catalytic activity of the first partial reaction (adenylation), leaving the second step unaffected, and it is reversed by a sirtuin deacetylase [25,26].

The present study aims to characterize *E. coli* Acs kinetics and thermodynamics. A structural model for the adenylating conformation, not available so far, was predicted using other ANL enzyme structures as templates. From the Acs model, four amino acids were selected to study their role in catalysis and ATP-binding: T264, K270, D500 and K609. The results evidenced to the important role of these residues in the catalytic ability and ATP-binding of Acs enzyme.

2. Methods

2.1 Plasmids construction and incorporation of N-(Ɛ)-acetyl-lysine into Acs at K609

To overexpress Acs protein (uniprot code P27550), the corresponding ASKA plasmid was used (ASKA*acs*) [27]. Overexpression plasmids of the single amino acid mutants of Acs (T264A, K270A, D500A and K609A) were obtained by site-directed mutagenesis from ASKA*acs* plasmid (ASKA*acs*^{T264A}, ASKA*acs*^{K270A}, ASKA*acs*^{D500A}, ASKA*acs*^{K609A}). To purify CobB deacetylase protein, the gene *cobB* of *E. coli* BW25113 was PCR-amplified and cloned into pBAD24-MBP [28]. To overexpress Acs protein acetylated on K609 (K609Kac), incorporation of N-(Ɛ)-acetyl-lysine was carried out using the genetic code expansion concept. A pRSF-Duet-1 modified plasmid for site-specific incorporation of acetyl-L-lysine (pRSF-Duet-1- acetyl-lysyl-tRNA-synthetase AcKRS3/M*b*tRNA$_{CUA}$), kindly supplied by Prof. Michael Lammers (University of Cologne) was employed [29,30]. *acs* gene containing an amber stop codon at the 609 position was constructed by site-directed mutagenesis from ASKA*acs* plasmid. His6-*acs*K609ambercodon gene was PCR-amplified and cloned into pRSF-Duet-1- acetyl-lysyl-tRNA-synthetase AcKRS3/M*b*tRNA$_{CUA}$ plasmid (pRSF*acs*^{K609ac}). All molecular biology enzymes used were purchased from Thermo Fisher Scientific. The strains, plasmids and primers used are listed in Supplementary Table S1.

2.2 Proteins overexpression and purification

Chemically competent *E. coli* BL21 (DE3) strains were transformed by heat shock at 42 °C with overexpressing plasmids. Cultures were grown overnight at 30 °C with orbital shaking (200 rpm). The culture medium was lysogen broth (LB) (10 g L^{-1} tryptone, 5 g L^{-1} yeast extract and 5 g L^{-1} NaCl). Expression was induced with 0.1 mM Isopropyl β-D-1-thiogalactopyranoside (IPTG) when the culture optical density at 600 nm (OD_{600}) reached 0.5-0.6. To obtain site-specifically acetylated Acs (Acs K609ac), overexpression cultures were supplemented with 10 mM L-acetyl Lysine and 20 mM nicotinamide (Sigma Aldrich) after IPTG induction. Cell pellets were harvested by centrifugation (20 min; 6000 x g) and resuspended in binding buffer (50 mM potassium phosphate, 500 mM NaCl, 25 mM imidazole, pH 8). Cells were disrupted by three passages of the crude extract through a French pressure cell system at 20,000 psi. Following the removal of cell debris by centrifugation at 18000 x g for 30 min at 4 °C, the supernatant was applied onto a Ni (II)-loaded 5 mL His-Trap HP column (GE Heathcare) previously equilibrated in binding buffer. Protein was eluted using a linear gradient of imidazole from 0 to 500 mM at a flow rate of 5 mL min^{-1}. The protein buffer was then changed to buffer A (50 mM Tris-HCl, 2 mM dithiothreitol (DTT), pH 7.4) using a HiPrep™ 26/10 desalting column (GE Heathcare) at a flow rate of 5 mL min^{-1}. The final Acs fractions were then concentrated

and further purified using a Superdex 75 10/300 GL gel filtration column (GE Heathcare) equilibrated with buffer B (100 mM Tris-HCl, 150 mM NaCl, 1 mM TCEP, 3 mM $MgCl_2$, pH 7.4) at a flow rate of 0.5 mL min^{-1}. CobB sirtuin was purified using an amylose resin (New England Biolabs) following a previously reported protocol [28].

2.3 Protein deacetylation

Selected proteins were deacetylated with CobB sirtuin. The reactions were carried out with a 1:50 ratio (Acs:CobB) in the presence of 2 mM NAD^+ at 30 ^oC for 8 hours [28]. To separate Acs and CobB proteins, reactions were loaded onto a 5 ml Hi-trap Q HP (GE Heathcare) column anionic exchange column, at a flow rate of 5 mL min^{-1} previously equilibrated with buffer A. A step gradient procedure was used to separate the proteins with increasing ionic strength from 0 to 1 M NaCl.

2.4 Liquid chromatography–mass spectrometry assay (LC-MS)

To evaluate acetylation level of Acs, purified Acs before and after (deacetylated Acs, deacAcs) CobB incubation, and Acs K609ac, were analysed by LC-MS. Samples were alkylated by incubation with 100 mM iodoacetamide (IAA) for 30 min at room temperature in the dark. Proteins were digested with 0.5–1 µg of proteomics grade Trypsin Gold (Promega) for 3 h at 37 ˚C. The reaction was stopped by the addition of 0.1% formic acid, and the samples were dried using a vacuum evaporator. Tryptic peptides generated from the samples were separated and analysed by LC-MS. An Agilent 1100 (Agilent Technologies) was equipped with a Zorbax SB-C18 HPLC column (Agilent Technologies) and connected to an Agilent Ion Trap XCT Plus mass spectrometer (Agilent Technologies) that had an electrospray (ESI) interface. Two mobile phases were used: phase A was composed of water/acetonitrile/ formic acid (94.9:5:0.1, v/v), and phase B consisted of water/acetonitrile/formic acid (10:89.9:0.1, v/v). The digested peptides were resuspended in 20 µl of phase A and eluted using a linear gradient of 0–80% phase B for 180 min at a flow rate of 10 µl min^{-1}. The mass spectrometer was operated in positive mode with a capillary spray voltage of 3500 V, at a scan speed of 8100 (m/z)/sec from 50 to 2200 m/z, with a target mass of 1000 m/z, and three scans were averaged. The nebulizer gas pressure was set at 15 psi, and the drying gas flowed at 5 L min^{-1} at a temperature of 350˚C. MS/MS data were collected in an automated data-dependent mode (AutoMS mode). Data processing was performed with the Data Analysis program for LC/MSD Trap Version 3.3 (Bruker Daltonik) and the Spectrum Mill MS Proteomics Workbench (Agilent Technologies) [60,61]. After automated validation of the results, the identified proteins and the sequences of the

digested peptides were compiled. Peptides with a score threshold of 8 and a percentage-scored peak intensity higher than 70% were considered valid.

2.5 Circular dichroism

Circular dichroism spectroscopy (CD) was performed on a PiStar-180 spectrophotometer (Applied Photophysics, U.K.) equipped with a N_2 purge and a Peltier system for temperature control. Far-UV CD spectra (190-240 nm) were obtained at 20 °C from protein samples (0.15 mg mL^{-1}) in 50 mM potassium phosphate buffer pH 7.4 containing 20 mM NaCl). The spectra were obtained in a 0.1 cm path length cuvette, reading every nm. Data were converted to molar ellipticity units by using the mean residue mass of 110.40 kDa.

2.6 Kinetics characterization

The acetyl-CoA synthetase assay was based on the coupled assay reported by Williamson and Corkey [31]. AMP production was detected *via* a coupled enzyme assay in which myokinase (MK), pyruvate kinase (PK) and lactate dehydrogenase (LDH) couple AMP production to NADH oxidation. Standard acetyl-CoA synthetase assays (0.2 mL) were performed at 37 °C in 50 mM potassium phosphate buffer at pH 7.5 containing 3.0 mM PEP (phosphoenolpyruvate), 5 units MK, 1 unit PK, 1.5 units LDH, 5 mM MgCl2, 2.5 mM ATP, 1.5 mM CoA, 0.1 mM NADH, 5 mM acetate and 1 mM DTT. The reaction was started by the addition of Acs. All reactions were performed in triplicate. Specific activity was calculated using the extinction coefficient of NADH (6.22 mM^{-1} cm^{-1}) and was based on the oxidation of two molecules of NADH for each AMP molecule released. One unit of Acs activity is defined as 1 µmole of acetyl-CoA formed per minute at pH 7.5 and 37 °C. Obtained milliunits of absorbance per minute at 340 nm (Synergy H1 Hybrid Multi-Mode Reader, Biotek), were converted to units of absorbance per minute by means of the PathCheck Sensor feature. Substrate concentrations were varied from 0 to 0.5 mM for ATP and 0 to 2 mM for acetate. Pseudo-first-order kinetic parameters were determined using Prism v6 (GraphPad) analytical software and standard deviations were determined from the three replicates. Statistical multiple comparison one-way ANOVA has been carried out for kinetic parameters to know if the differences between parameters were or not significatively different. Acs inhibition assays were carried out employing a pyrophosphate detection kit (Sigma Aldrich) following the commercial protocol.

2.7 Isothemal titration calorimetry assays

To determine the thermodynamic parameters of interaction between Acs proteins and ATP, isothermal titration calorimetry (ITC) assays were carried out using a VP-ITC micro-calorimeter (MicroCal). Protein was inserted in the cell at a concentration of 70 µM, while the ligand concentration in the syringe was at 800 µM. Titrations were performed at 25 °C with 30 injections of 10-µL each, separated by 5 min, into the 2 ml sample cell. Data were fitted to a one-binding-site model using Peaq-ITC software (Malvern). Each binding isotherm was measured at least in duplicate and standard deviations were determined from the two replicates. Statistical multiple comparison one-way ANOVA has been carried out for thermodynamic parameters to know if the differences between parameters were or not significatively different.

3. Results

3.1 Acs structural model

To ascertain the 3D disposition of the residues involved in the adenylating step performed by *E. coli* Acs, structural models were built using SWISS-MODEL software [32], using ten ANL structures in the adenylating conformation as templates. The quality parameters of the models are summarized in Supplementary Table S2. On the basis of the QMEAN and GMQE values [33], the model generated with the acyl-CoA synthetase from *Saccharomyces cerevisiae* (PDB ID: 1RY2) as template was selected [8]. The model showed a z-score QMEAN of -2.55 and was compared to 1RY2 template through structural alignment. The structures were essentially identical (Figure 2A2) and conserved lysine from A10 motif was located at the same position (Figure 2A3).

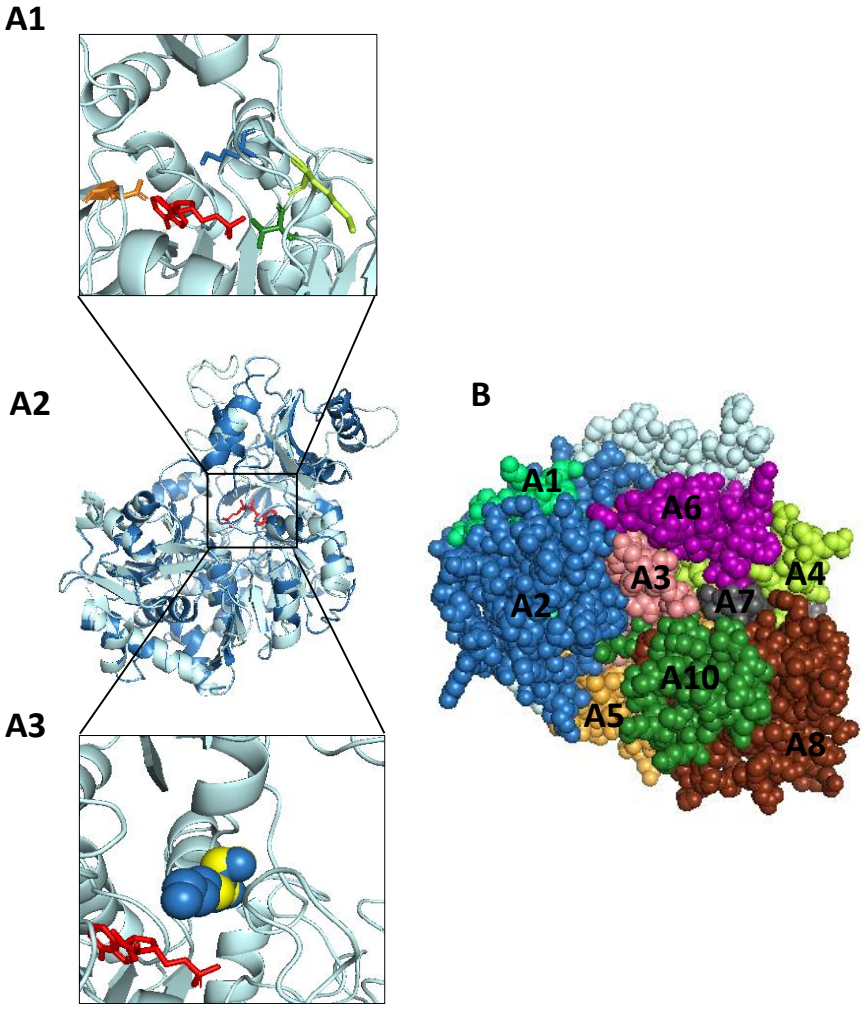

Figure 2. *E. coli* Acs model generated using medium chain acyl-CoA synthetase from human mitochondria. **(A1)** Selected residues (K609 in blue, T264 in green, K270 in yellow, and D500 in orange) surrounding ATP (red) ligand. **(A2)** Model (light blue) aligned with target structure (dark blue). **(A3)** Conserved A10 lysines, K609 from model (blue) and K557 from target (yellow) and ATP ligand (red). **(B)** Conserved ANL family motifs A1-A10 (ATP substrate is in red). Figure was made using PyMOL Molecular Graphics System, Version 2.0 Schrödinger, LLC.

3.2 Effects of single amino acid substitutions on Acs structure

To identify the conserved residues in the ANL sequences, the *E. coli* Acs sequence was aligned with the sequences of ANL proteins from different organisms whose structures had been previously determined in the closed conformation (these structures were also used to construct Acs model): acetyl-CoA synthetase from *Sacharomyces cerevisiae*, medium chain acyl-CoA synthetase from human mitochondria, 4-coumarate:CoA ligase from *Nicotiana tabacum*, malonyl CoA synthetase (MatB) from *Rhodopseudomonas palustris*, acyl-CoA synthase (FadD32) from *Mycobacterium*

smegtatis, 2-succinylbenzoate-CoA ligase (MenE) from *Bacillus subtilis* and D-alanyl carrier protein ligase (DltA) from and *Bacillus cereus* (Figure 3) [8–12,16,26,34,35]. Identity percentages were 48%, 26 %, 23 %, 23 %, 25 %, 20% and 27 %, respectively. From protein alignment, 3D model and previous literature [8–12,16,26,34,35], four residues were selected from the Acs *E. coli* sequence to study their role in Acs catalytic mechanism: threonine 264 (T264) and lysine 270 (K270) from A3 motif P-loop, aspartic acid 500 (D500) from A7 motif and lysine 609 (K609) from A10 motif (Figure 3).

Figure 3. Protein alignment. Selected residues to single substitutions (yellow box) are shown.

The selected residues were mutated to alanine with site-directed mutagenesis, producing single Acs mutants, which were deacetylated *in vitro* by CobB after purification: Acs T264A, Acs K270A, Acs D500A and Acs K609A. The proteins were analysed by CD in order to investigate the effect of the substitutions and acetylation on the conformation of Acs. The α-helical content was also determined using the software Bestsel [36,37] (Table 1). As shown in Figure 4, the spectra for the single mutants were very similar to the spectrum of the native Acs, indicating the absence of major structural changes induced by mutations. Quantitative analysis of α-helical content indicated a relative amount from 12.2 to 13.8 %, also suggesting that the Acs structure was not affected by the mutations. On the other hand, site-specific K609 acetylation produced a

protein (Acs K609ac) with a significant increase of the α-helical content (22.3%), suggesting an impact of this protein modification onto the Acs protein structure.

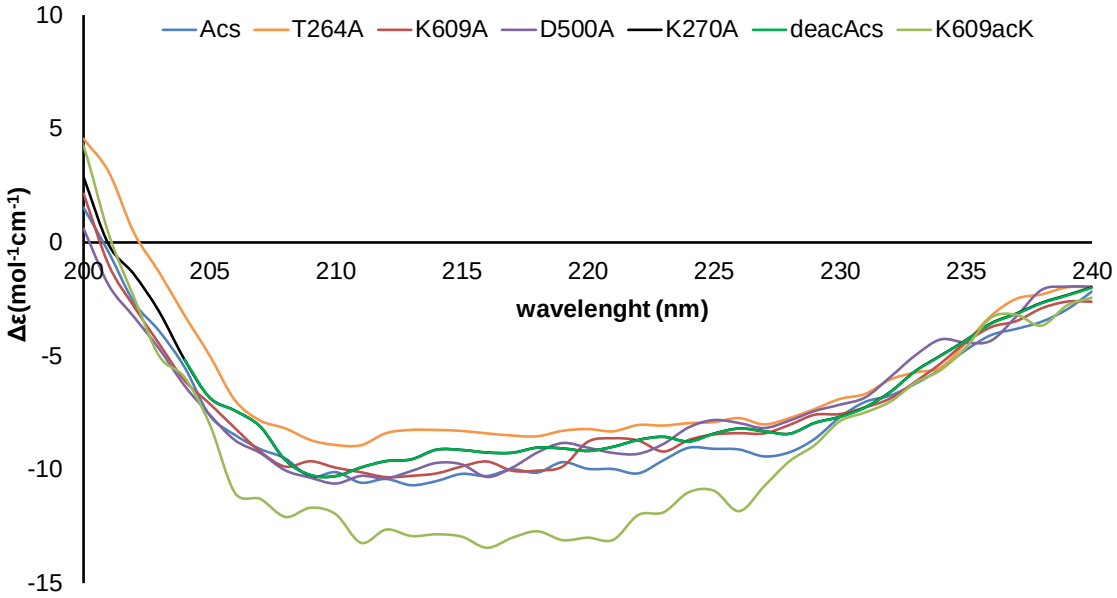

Figure 4. Far UV spectra of proteins. The color code is indicated in the figure.

Table 1. α-helical content of Acs proteins.

	deacAcs	Acs	T264	K270	D500	K609	K609ac
Helical content (%)	13.4	13.1	12.2	13.1	13.8	12.2	22.3

3.3 Effects of single amino acid substitutions on Acs activity

Acs protein purified from *E. coli* BL21 (DE3) showed 14 acetylated Lys (K11, K106, K115, K123, K130, K207, K221, K408, K416, K585, K604, K609, K617, K640), as verified using liquid chromatography mass spectrometry (LC-MS/MS). Wild-type and mutants were incubated with CobB and NAD^+, and LC-MS/MS showed that eight acetylated Lys (K106, K123, K130, K207, K221, K585, K604 and K617) were maintained, while K11, K115, K408, K416, K609 and K640 were deacetylated by CobB, suggesting that they are site-specific substrates of CobB deacetylase (Table 2). *In vitro* acetylation of K609 to produce

K609ac followed by LC-MS/MS, produced six acetylated Lys (K123, K130, K408, K604, K609 and K617).

Table 2. Acs LC-MS/MS assay. Site-specific lysine deacetylation of Acs by CobB is shown in bold. Acetylated lysines not detected previously are shown in italic.

	Acs	**deacAcs**
Acetylated lysines	14 (***K11***, K106, ***K115***, *K123*, K130, K207, K221, **K408**, **K416**, K585, K604, **K609**, K617 and **K640**)	8 (K106, K123, K130, K207, K221, K585, K604 and K617)

Kinetics characterization of Acs and its mutants was carried out using ATP and acetate substrates. Michaelis-Menten behaviors were observed for all the proteins and substrates. Kinetic parameters are summarized in Table 3.

Deacetylated Acs showed a K_M value of 73 and 35 µM for ATP and acetate, respectively. Acetylation did not affect to the K_M values (76.32 and 41 µM for Acs without deacetylation), while it strongly affected the k_{cat} values, being 6900 and 4600 min^{-1} for ATP and acetate in the deacetylated form, and 52.23 and 38.26 min^{-1} for the acetylated form. T246A and D500A mutations decreased both K_M and k_{cat} values: specificity constants (k_{cat}/K_M) for T264A mutant dropped of 36 and 43-fold for ATP and acetate substrates respectively, while k_{cat}/K_M for D500A mutant protein decreased 3200 and 2500-fold for ATP and acetate, respectively. Surprisingly, mutation of K270 produced an increase of 8 times for ATP and 6 times for acetate as compared to the native Acs, while the K_M values were similar to native Acs. Finally, K609A and K609Kac proteins did not show any activity.

Table 3. Kinetic parameters for Acs and mutant proteins with ATP and acetate as substrates.

	deacAcs	**Acs**	**T264A**	**K270A**
K_M ATP (µM)	73 ± 8	80 ± 10	330 ± 50	65 ± 3
k_{cat} ATP (min^{-1})	6900 ±800	52 ± 6	900.25 ± 82	6000 ± 1000
K_M acetate (µM)	35 ± 2	41 ± 2	350 ± 20	25 ± 1
k_{cat} acetate (min^{-1})	4600 ± 600	39± 6	1080 ± 50	29000 ±1000
k_{cat}/K_M ATP (min^{-1} μM^{-1})	95.28	0.68	2.67	870

k_{cat}/K_M acetate (min^{-1} μM^{-1})	132.05	0.93	3.08	1177
	D500A	**K609A**	**K609ac**	
K_M ATP (μM)	270 ± 10	Inactive	Inactive	
k_{cat} ATP (min^{-1})	8.2 ± 0.3	Inactive	Inactive	
K_M acetate (μM)	1600 ± 80	Inactive	Inactive	
k_{cat} acetate (min^{-1})	8.6 ± 0.3	Inactive	Inactive	
k_{cat}/K_M ATP (min^{-1} μM^{-1})	0.03	Inactive	Inactive	
k_{cat}/K_M acetate (min^{-1} μM^{-1})	0.0053	Inactive	Inactive	

3.4 Effects of single amino acid substitutions on ATP binding by Acs

The thermodynamics of ATP-binding to Acs proteins were studied using ITC. Titration of ATP onto acetylated and deacetylated proteins produced endothermic peaks indicative of the occurrence of protein-ligand interaction (Figure 6). A fitting of the binding isotherms indicates that one ATP molecule binds per protein monomer, with a dissociation constant of 30 μM (deacAcs, Figure 6A) and 50 μM (Acs, Figure 6B). The binding is entropy-driven, showing a positive favourable ΔS ($T\Delta S$ = 86.3 kJ mol^{-1} K^{-1} for deacAcs and 31.6 kJ mol^{-1} K^{-1} for Acs) and a positive unfavourable enthalpy (ΔH = 10 kJ mol^{-1} for deacAcs and 7 kJ mol^{-1} for Acs) (Table 4). No-binding was observed when acetate was titrated into a sample cell containing Acs alone (Supplementary Figure S1), indicating that Acs interacts with its organic acid substrate only in the ATP-bound form.

K609A (Figure 6C) and K270A (Figure 6D) Acs mutants bind ATP with an endothermic reaction, as observed for the native protein. The K609A mutant (Figure 6C) binds ATP with the highest affinity, with a K_d of 3.55 μM, one order of magnitude lower than the one measured for the native protein, the highest value of ΔH 16.5 kJ mol^{-1} and $T\Delta S$ = 47.7 kJ mol^{-1} K^{-1} (Table 4). The K270A mutant, on the other hand, showed a similar affinity to the native protein with K_d of 20 μM, and lower values of ΔH = 2.7 kJ mol^{-1} and $T\Delta S$ = 29.6 kJ mol^{-1} K^{-1}. On the other hand, D500A (Figure 6E) and T264A (Figure 6F) mutations produced Acs variants unable to bind ATP.

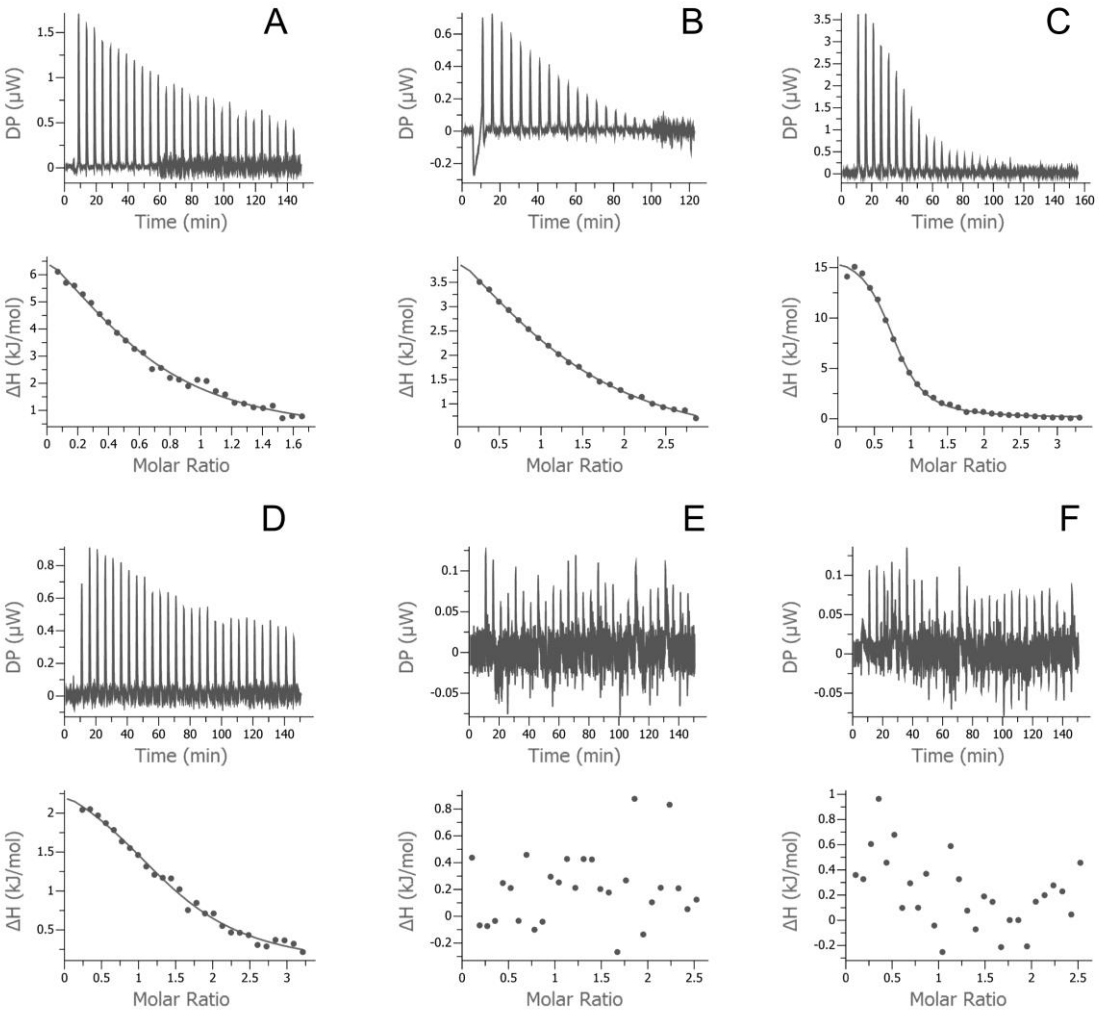

Figure 6. ATP titrations onto deacAcs **(A)**, Acs **(B)**, K609A **(C)**, K270A **(D)**, T264A **(E)** and D500A **(F)**, followed by ITC. Raw data of heat flow as a function of time (top panels) and integrated data after subtraction of the heat of dilution (bottom panels) are reported. The solid lines represent the best-fit curves to the data, using a single-set-of-site model.

Differently from the deacetylated proteins, injections of ATP onto K609ac solution produced an exothermic response. A fit of the binding isotherm indicated that ATP binds K609ac protein with higher affinity, as compared to the deacetylated proteins, with K_d of 2.07 µM, a negative favorable ΔH = -131 kJ mol^{-1} and a negative unfavorable $T\Delta S$ = -98.4 kJ mol^{-1} K^{-1} (Table 4).

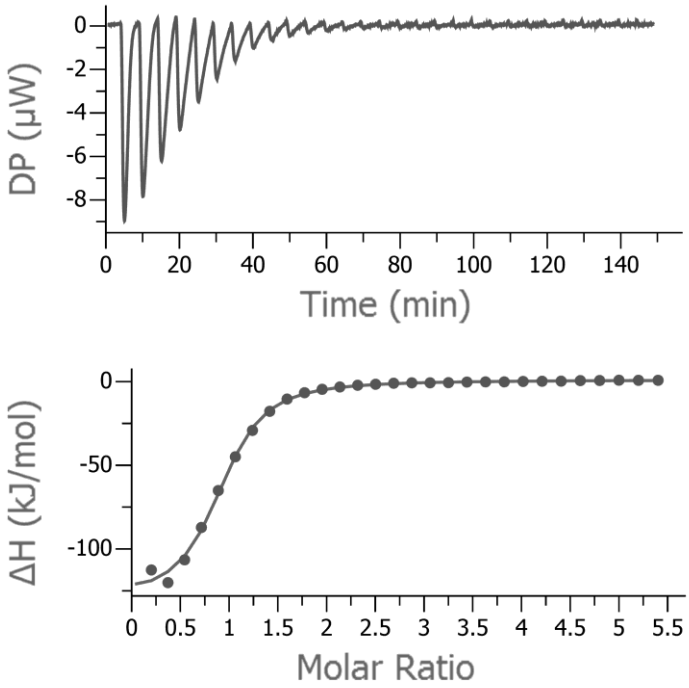

Figure 7. ATP-binding to K609ac Acs protein followed using ITC. Raw data representing heat flow over time are reported (top panel) together with integrated head data after subtraction of the heat of dilution (bottom panel). The solid line represents the best-fit of the data, using a one-set-of-sites binding model.

Table 4. Thermodynamic parameters of ATP-binding for Acs wt and mutant proteins. K_d: dissociation constant, ΔH: enthalpy change, ΔS: entropy change.

	deacAcs	**Acs**	**K609A**	**270A**	**K609ac**
Kd (µM)	30 ±10	50 ± 10	3.55 ± 0.01	20 ± 6	2.07 ± 0.01
ΔH (kJ mol^{-1})	10 ± 2	7 ± 1	16.5 ± 0.4	2.7 ± 0.3	-131 ± 3
TΔS (kJ mol^{-1} K^{-1})	86.3	31.6	47.7	29.6	-98.4

3.5 Acs inhibition by cAMP

S. enterica Acs inhibition by cAMP has been recently reported [38]. To verify if *E. coli* Acs was similarly inhibited by cAMP and AMP, enzymatic reactions were carried out in the presence of 1 mM cAMP or AMP. cAMP was able to inhibit Acs, while no inhibition was observed when AMP was present (Figure 8). To determine the inhibition constant (k_i) of cAMP, apparent K_M were determined at different cAMP concentrations from 0 to 1 mM (0, 50, 500 and 1000 µM) and plotted *versus* inhibitor concentration (Figure 8A). The calculated value of k_i was 232 µM. Moreover, a double-reciprocal plot (1/v *versus* 1 /

[ATP]) at different cAMP concentrations was built (Figure 8B), suggesting the occurrence of a competitive inhibition mechanism, as previously described for *S. enterica* Acs [38].

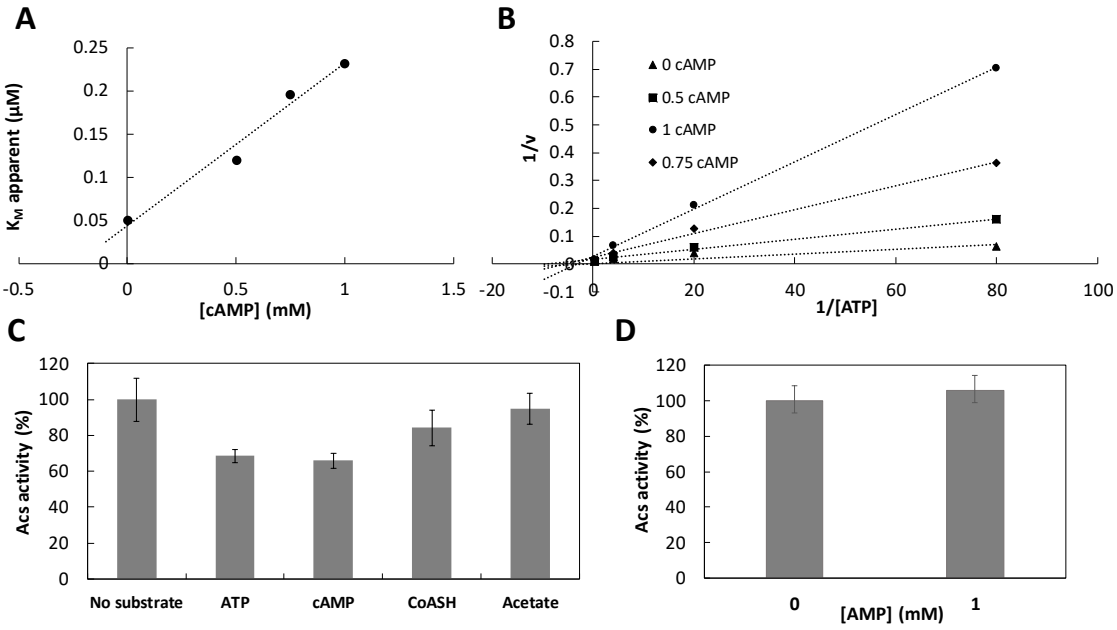

Figure 8. Analysis of CobB inhibition by cAMP. **(A)** Acs apparent K_M at different cAMP concentrations. **(B)** Double-reciprocal plot (1/v *versus* 1/ ATP]) of Acs activity at different cAMP concentrations: 0 (▲), 0.5 (■), 0.75(♦) and 1 (•) μM. **(C)** Acs activity (%) after CobB deacetylation in the absence or in the present of ATP, cAMP, CoA or acetate. **(D)** Acs activity (%) in the absence and in the presence of AMP 1mM. Presented data are average of triplicates. Standard deviations were always less than 10%

To ascertain whether the presence of substrates or cAMP inhibitor affected Acs deacetylation by CobB, as observed for *S. enterica* Acs, deacetylation assays using Acs as substrate were carried out in the presence of 1 mM ATP, cAMP, CoA or acetate. Acs activity was measured after deacetylation, and the activity was compared with a control assay without substrate or inhibitor (Figure 8C). Acs deacetylation by CobB is partially inhibited in the presence of ATP and cAMP, while it is not affected by the presence of acetate or CoA.

Acs-cAMP binding was studied by ITC for all the proteins. Calorimetric assays were carried out under the same conditions employed for ATP-binding studies, but no-binding was observed under the conditions tested (data not shown).

4. Discussion

ANL enzymes belong to a superfamily of proteins essential for the metabolism of all organisms, from bacteria to humans. Acs protein has a principal role in *E. coli* acetate

metabolism, catalysing one of the acetate uptake pathways. *E. coli* is the most used microorganism in biotechnology, and acetate excretion limits growth rates and bioprocess yields [39,40]. Thus, the understanding of the acetate metabolism is important to optimize the biotechnological systems based on *E. coli* metabolism.

ANL dynamic conformation is an atypical characteristic of this family of enzymes. Several ANL enzymes have been resolved in the thioester-forming or open conformation [41–45], but less information is available about the adenylating or closed conformation. To our knowledge, ten proteins have been crystalized in this conformation [8–16,35]. In this study we used these structures as templates to predict models of *E. coli* Acs protein in the closed conformation. The model with least z-score was selected and was aligned with the template structure to locate conserved positions. This allowed us to select four residues which were located around the ATP substrate (Figure 2A1), two of them (T264 and K270) belonging to P-loop from A3 motif, which has a similar sequence than those from ATPases and GTPases [46] and has been found wrapping ATP pyrophosphate in several ANL structures [8–11,13,14]. In addition, D500 is a 100% conserved ANL residue from the A7 motif involved in ATP-binding through ribose sugar moiety [9,11,14,16] and K609 lies in the A10 motif and is involved in adenylating catalytic step being found to interact with the α-phosphate [11,13,16,47,48], the β-phosphate [8,9] or both of them [10] of the ATP substrate. The role of K609 residue has been widely studied for several ANL enzymes showing a great decrease or a null activity when this residue is mutated [7,13,25,28,45,49–51]. Thus, Reger *et al*. reported a total loss of activity of *Salmonella enterica* Acs when this residue was mutated by alanine [45]. The acetylation of the A10 conserved lysine has been described as a regulator mechanism in many ANL enzymes [19,21,35,52,53]. Thus, in *E. coli*, Acs activity is regulated *in vivo* by acetylation/deacetylation, which constitutes an acetate metabolism regulation system [28,54]. Acs is acetylated by PatZ acetyltransferase (also known as Pka or YfiQ) in several lysines, although, to date, K609 is the only one responsible for Acs activity regulation. K609 acetylation induces Acs inhibition [24], which is reversed by CobB sirtuin [28]. In this study 14 acetylated lysines were observed in Acs sequence and six of these lysines were identified as CobB substrates (K11, K115, K408, K416, K609 and K640). This result agrees with our previous work which demonstrated that CobB deacetylates several acetylated Lys in Acs sequence, not only K609. Moreover, LC-MS assay identified six lysines acetylated in Acs sequence that had not been observed previously (K11, K115, K123, K408, K416 and K640) [55–60].

Acs kinetics were determined for the Acs native enzyme and for the single amino acid selected mutants. Native Acs kinetic parameters were similar to those reported for other ANL enzymes, with a K_M in the range of 20-100 µM. However, k_{cat} values were much higher than those previously reported [6,9,12,13,15,16,26,45,49,61]. ANL k_{cat} determined to date are between 10-2000 min^{-1}, whereas our Acs k_{cat} was 6900 and 4600 min^{-1} for ATP and acetate, respectively. These high values could be due to protein deacetylation after purification. Kinetic parameters measured for Acs without deacetylation showed no change of enzyme specificity (K_M), but a significant reduction of activity (k_{cat}). This result suggests that acetylation decreases the amount of active enzyme through enzyme inhibition, although it does not affect substrates specificity. Acs deacetylation increased k_{cat} values more than a 100-fold. Thus, protein deacetylation is essential to study Acs activity and single amino acids substitutions, although, to our knowledge, this is the first kinetic study of an ANL enzyme previously deacetylated to ensure that all the protein is catalytically active.

The kinetic parameters of mutant proteins showed differences with respect to native Acs. Acs D500A protein showed a 3.69 and 45-fold increase for ATP and acetate K_M, respectively. The catalytic response of an ANL enzyme to this conserved aspartic acid mutation has been previously reported. Thus, a 75-fold and 500-fold increase in the K_M values for ATP were observed for DltA enzyme from *B. cereus* and 4CBL (4-chlorobenzoate: Coenzyme A ligase) from *Alcaligenes* sp*,* respectively, when this residue was mutated [7,9]. Wu et al., suggest that, although the conserved aspartic is not near acyl- binding pocket, its role may be important for the second step of the 4CBL protein [7]. T264 replacement by alanine induced an important change in Acs catalytic response. K_M values were 4.6 and 10 times higher than native values for ATP and acetate, respectively. The catalytic role of T264 (first residue in P-loop) has previously been studied and similar catalytic effects were described [7,11]. K_M values for K270A mutant were very similar to those observed for native Acs; however, k_{cat} values were much different. K270A mutant showed a surprising increase in the k_{cat} constants (almost 10-fold). To our knowledge, the catalytic role of this residue has not been studied to date. From our results we suggest that this residue may have an important catalytic role in Acs reaction that had not been shown before.

Acs proteins (Acs and deacAcs) showed very similar thermodynamic parameters, suggesting that *in vivo* Acs acetylation does not affect ATP-binding. The values of dissociation constants (30 and 50 µM) are similar to those determined for the

Rhodopseudomonas palustris (*R. palustris*) malonyl-CoA synthetase (MatB) protein (5.6 µM) [12] and *Mycobacterium smegtatis* (*M. smegtatis*) FadD32 protein (35 µM) [14], and were lower than that reported for *S. enterica* Acs (322 µM) [38]. Kd values measured by ITC are in the same order of magnitude as the ATP K_M determined in this study, 73 and 76.32 µM, respectively. Acs K270A mutant protein showed a Kd for ATP-binding very similar to native Acs, as was observed when ATP K_M were compared. K609A mutant protein showed a larger enthalpy of reaction and a lower dissociation constant (3.55 µM). A similar behavior was observed by Crosby et al. (2012) for the *R. palustris* MatB protein [12]: MatB, a protein of ANL family, showed a lower affinity and binding enthalpy as compared to its mutant in the A10 conserved lysine [12].

To study the effect of K609 acetylation in ATP-binding, an Acs version specifically acetylated in K609 was constructed and purified. Circular dichroism results showed that Acs K609ac had a different conformational fold from the others Acs proteins, as well as a changed behaviour for ATP-binding, with a higher affinity and opposite binding signatures ΔH and ΔS. This result again points out the importance of this residue in Acs catalytic mechanism which is reflected in the enzyme inhibition by K609 acetylation. The diverse ATP-binding mode of the K609ac protein reflects a change in the catalytic reaction: in particular, the higher affinity of this protein variant for ATP. It is important to note that, according to MS results, both acetylated and deacetylated molecules of Acs co-exist in the protein preparation. Thus, MS spectrometry showed K609 in the acetylated and deacetylated states for Acs protein. This observation could reflect that Acs showed a behavior very similar to deacetylated Acs and different from K609ac protein.

Competitive inhibition of *S. enterica* Acs by cAMP has been recently demonstrated [38], so we decided to study *E. coli* Acs inhibition. An inhibition constant of 232 µM was established. This value was very similar to those determined for *S. enterica* Acs (185 µM) and intracellular cAMP concentration calculated for *E. coli* grown in the absence of glucose [62,63]. Acs-cAMP binding was studied by ITC. However, no-binding was observed under the conditions tested, indicating a low binding affinity which is coherent to the ki measured for cAMP, which is almost 10 times higher than the dissociation constant for ATP. The presence of cAMP and ATP hindered CobB deacetylation. This result was also observed for *S. enterica* Acs in the presence of cAMP and the authors suggested that Acs-CobB binding could induce a different Acs conformation and the presence of cAMP, which might hinder the formation of this conformation. Further

investigation is necessary to confirm this suggestion, which would suppose a new level of regulation of Acs deacetylation by CobB depending on cAMP and ATP intracellular concentrations.

In conclusion, this work studies for the first time the *E. coli* Acs ATP-binding parameters and the role of four important conserved residues. Thus, the effect of K609 mutation on ATP-binding observed in this study opens a new research field for understanding how acetylation induces enzyme inhibition.

5. Acknowledgements

Dr. Michael Lammers (Institute of Biochemistry, Synthetic and Structural Biochemistry, University of Greifswald, Greifswald, Germany) is acknowledged for pRSF-Duet-1-acetyl-lysyl-tRNA-synthetase AcKRS3/M*bt*RNA$_{CUA}$ plasmid transference. Dr. Alejandro Torrecillas (CAID, University of Murcia) is acknowledged for technical support.

6. Funding

This work was supported by grants from the MICINN BIO2014-54411-C2-1-R, which includes ERDF European cofounding, and the Seneca Foundation CARM (19236/PI/14).

7. CRediT author statement

Julia Gallego-Jara: conceptualization, methodology, investigation, writing-original draft. Gema Lozano Terol: methodology, investigation. Ana Écija Conesa: methodology, investigation. Barbara Zambelli: conceptualization, methodology, investigation, writing – review and editing, supervision and visualization. Manuel Cánovas Díaz: writing – review and editing, project administration, funding acquisition. Teresa de Diego Puente: conceptualization, investigation, writing – review and editing, supervision, project administration, funding acquisition.

8. References

1. Gulick AM. Conformational dynamics in the acyl-CoA synthetases, adenylation domains of non-ribosomal peptide synthetases, and firefly luciferase. ACS Chem Biol. 2009;4: 811–827. doi:10.1021/cb900156h

2. Berg P. Acyl adenylates: an enzymatic mechanism of acetate activation. J Biol Chem. 1956;222: 991–1013.

3. Farrar WW, Plowman KM. Kinetics of acetyl-CoA synthetase-I. Mode of addition of substrates. Int J Biochem. 1975;6: 537–542. doi:10.1016/0020-711X(75)90069-5

4. Tian Y, Suk D-H, Cai F, Crich D, Mesecar AD. *Bacillus anthracis* O-succinylbenzoyl-CoA synthetase: reaction kinetics and a novel inhibitor mimicking its reaction intermediate. Biochemistry. 2008;47: 12434–12447. doi:10.1016/j.neuron.2009.10.017.A

5. Kim YS, Kang SW. Steady-state kinetics of malonyl-CoA synthetase from *Bradyrhizobium japonicum* and evidence for malonyl-AMP formation in the reaction. Biochem J. 1994;297: 327–333. doi:10.1042/bj2970327

6. Li H, Melton EM, Quackenbush S, DiRusso CC, Black PN. Mechanistic studies of the long chain acyl-CoA synthetase Faa1p from *Saccharomyces cerevisiae*. Biochim Biophys Acta - Mol Cell Biol Lipids. 2007;1771: 1246–1253. doi:10.1016/j.bbalip.2007.05.009

7. Wu R, Cao J, Lu X, Reger AS, Gulick AM, Dunway-Mariano D. Mechanism of 4-chlorobenzoate: Coenzyme A ligase catalysis. Biochemistry. 2008;47: 8026–8039. doi:10.1021/bi800698m

8. Kochan G, Pilka ES, von Delft F, Oppermann U, Yue WW. Structural snapshots for the conformation-dependent catalysis by human medium-chain acyl-Coenzyme A synthetase ACSM2A. J Mol Biol. 2009;388: 997–1008. doi:10.1016/j.jmb.2009.03.064

9. Osman KT, Du L, He Y, Luo Y. Crystal structure of *Bacillus cereus* D-alanyl carrier protein ligase (DltA) in complex with ATP. J Mol Biol. 2009;388: 345–355. doi:10.1016/j.jmb.2009.03.040

10. Law A, Boulanger MJ. Defining a structural and kinetic rationale for paralogous copies of phenylacetate-CoA ligases from the cystic fibrosis pathogen *Burkholderia cenocepacia* J2315. J Biol Chem. 2011;286: 15577–15585. doi:10.1074/jbc.M111.219683

11. Chen Y, Sun Y, Song H, Guo Z. Structural basis for the ATP-dependent configuration of adenylation active site in *Bacillus subtilis* O-succinylbenzoyl-Coa synthetase. J Biol Chem. 2015;290: 23971–23983. doi:10.1074/jbc.M115.676304

12. Crosby HA, Rank KC, Rayment I, Escalante-Semerena JC. Structure-guided expansion of the substrate range of methylmalonyl Coenzyme A synthetase (MatB) of *Rhodopseudomonas palustris*. Appl Environ Microbiol. 2012;78: 6619–6629. doi:10.1128/AEM.01733-12

13. Li Z, Nair SK. Structural basis for specificity and flexibility in a plant 4-coumarate:CoA ligase. Structure. 2015;23: 2032–2042. doi:10.1016/j.str.2015.08.012

14. Li W, Gu S, Fleming J, Bi L. Crystal structure of FadD32, an enzyme essential for mycolic acid biosynthesis in *Mycobacteria*. Sci Rep. 2015;5: 1–8. doi:10.1038/srep15493

15. Fan M, Xiao Y, Li M, Chang W. Crystal structures of *Arabidopsis thaliana* oxalyl-

CoA synthetase essential for oxalate degradation. Mol Plant. 2016;9: 1349–1352. doi:10.1016/j.molp.2016.06.002

16. Scaglione A, Fullone MR, Montemiglio LC, Parisi G, Zamparelli C, Vallone B, et al. Structure of the adenylation domain Thr1 involved in the biosynthesis of 4-chlorothreonine in *Streptomyces sp.* OH-5093—protein flexibility and molecular bases of substrate specificity. FEBS J. 2017;284: 2981–2999. doi:10.1111/febs.14163

17. Muller M. Energy metabolism of protozoa without mitochondria. Annu Rev Microbiol. 1988;42: 465–488. doi:10.1146/annurev.mi.42.100188.002341

18. Starai VJ, Escalante-Semerena JC. Acetyl-coenzyme A synthetase (AMP forming). Cell Mol Life Sci. 2004;61: 2020–2030. doi:10.1007/s00018-004-3448-x

19. Starai VJ, Celic I, Cole RN, Boeke JD, Escalante-Semerena JC. Sir2-dependent activation of acetyl-CoA synthetase by deacetylation of active lysine. Science (80-). 2002;298: 2390–2392. doi:10.1126/science.1077650

20. Gardner JG, Grundy FJ, Henkin TM, Escalante-Semerena JC. Control of acetyl-Coenzyme A synthetase (AcsA) activity by acetylation/deacetylation without NAD^+ involvement in *Bacillus subtilis*. J Bacteriol. 2006;188: 5460–5468. doi:10.1128/JB.00215-06

21. Crosby HA, Heiniger EK, Harwood CS, Escalante-Semerena JC. Reversible N-Lysine acetylation regulates the activity of acyl-CoA synthetases involved in anaerobic benzoate catabolism in *Rhodopseudomonas palustris*. Mol Microbiol. 2010;76: 874–888. doi:10.1111/j.1365-2958.2010.07127

22. Hayden JD, Brown LR, Gunawardena HP, Perkowski EF, Chen X, Braunstein M. Reversible acetylation regulates acetate and propionate metabolism in *Mycobacterium smegmatis*. Microbiology. 2013;159: 1986–1999. doi:10.1099/mic.0.068585-0

23. Schwer B, Bunkenborg J, Verdin RO, Andersen JS, Verdin E. Reversible lysine acetylation controls the activity of the mitochondrial enzyme acetyl-CoA synthetase 2. Proc Natl Acad Sci U S A. 2006;103: 10224–10229. doi:10.1073/pnas.0603968103

24. de Diego T, Gallego-Jara J, Castaño-Cerezo S, Bernal Sánchez V, Fernández Espín V, García de la Torre J, et al. The protein acetyltransferase PatZ from *Escherichia coli* is regulated by autoacetylation- induced oligomerization. J Biol Chem. 2015;53: 1689–1699. doi:10.1017/CBO9781107415324.004

25. Branchini BR, Murtiashaw MH, Magyar R a., Anderson SM. The role of lysine 529, a conserved residue of the acyl-adenylate- forming enzyme superfamily, in firefly luciferase. Biochemistry. 2000;39: 5433–5440. doi:10.1021/bi9928804

26. Horswill AR, Escalante-Semerena JC. Characterization of the propionyl-CoA synthetase (PrpE) enzyme of *Salmonella enterica*: Residue lys 592 is required for propionyl-AMP synthesis. Biochemistry. 2002;41: 2379–2387. doi:10.1021/bi015647q

27. Kitagawa M, Ara T, Arifuzzaman M, Ioka-Nakamichi T, Inamoto E, Toyonaga H, et al. Complete set of ORF clones of *Escherichia coli* ASKA library (a complete set of *E. coli* K-12 ORF archive): unique resources for biological research. DNA Res. 2005;12: 291–299. doi:10.1093/dnares/dsi012

28. Gallego-Jara J, Écija Conesa A, de Diego Puente T, Lozano Terol G, Cánovas Díaz M. Characterization of CobB kinetics and inhibition by nicotinamide. PLoS

One. 2017;12: e0189689. doi:10.1371/journal.pone.0189689

29. de Boor S, Knyphausen P, Kuhlmann N, Wroblowski S, Brenig J, Scislowski L, et al. Small GTP-binding protein Ran is regulated by posttranslational lysine acetylation. Proc Natl Acad Sci. 2015;112: E3679–E3688. doi:10.1073/pnas.1505995112

30. Kremer M, Kuhlmann N, Lechner M, Baldus L, Lammers M. Comment on 'YcgC represents a new protein deacetylase family in prokaryotes.' Elife. 2018;7: 1–12. doi:10.7554/eLife.37798

31. Williamson J, Corkey B. Assays of intermediates of the citric acid. In: Lowenstein J, Kaplan N, Colowick N, editors. Methods of Enzymology. Academic P. 1969. pp. 494–497.

32. Biasini M, Bienert S, Waterhouse A, Arnold K, Studer G, Schmidt T, et al. SWISS-MODEL: Modelling protein tertiary and quaternary structure using evolutionary information. Nucleic Acids Res. 2014;42: 252–258. doi:10.1093/nar/gku340

33. Benkert P, Biasini M, Schwede T. Toward the estimation of the absolute quality of individual protein structure models. Bioinformatics. 2011;27: 343–350. doi:10.1093/bioinformatics/btq662

34. Li Z, Nair SK. Structural basis for specificity and flexibility in a plant 4-coumarate:CoA ligase. Structure. 2015;23: 2032–2042. doi:10.1016/j.str.2015.08.012

35. Jogl G, Tong L. Crystal structure of yeast acetyl-Coenzyme A synthetase in complex with AMP. Biochemistry. 2004;43: 1425–1431. doi:10.1021/bi035911a

36. Micsonai A, Wien F, Bulyáki É, Kun J, Moussong É, Lee YH, et al. BeStSel: A web server for accurate protein secondary structure prediction and fold recognition from the circular dichroism spectra. Nucleic Acids Res. 2018;46: W315–W322. doi:10.1093/nar/gky497

37. Chen YH. Determination of the helix and β form of proteins in aqueous solution by circular dichroism. Biochemistry. 1974;13: 3350–3359. doi:10.1021/bi00713a027

38. Han X, Shen L, Wang Q, Cen X, Wang J, Wu M, et al. Cyclic AMP inhibits the activity and promotes the acetylation of acetyl-CoA synthetase through competitive binding to the ATP/AMP pocket. J Biol Chem. 2017;292: 1374–1384. doi:10.1074/jbc.M116.753640

39. Renilla S, Bernal V, Fuhrer T, Castaño-Cerezo S, Pastor JM, Iborra JL, et al. Acetate scavenging activity in *Escherichia coli*: interplay of acetyl-CoA synthetase and the PEP-glyoxylate cycle in chemostat cultures. Appl Microbiol Biotechnol. 2012;95: 2109–2124. doi:10.1007/s00253-011-3536-4

40. Valgepea K, Adamberg K, Vilu R. Decrease of energy spilling in *Escherichia coli* continuous cultures with rising specific growth rate and carbon wasting. BMC Syst Biol. 2011;5: 1–11. doi:10.1186/1752-0509-5-106

41. Chen Y, Jiang Y, Guo Z. Mechanistic insights from the crystal structure of *Bacillus subtilis* O-succinylbenzoyl-CoA synthetase complexed with the adenylate intermediate. Biochemistry. 2016;55: 6685–6695. doi:10.1021/acs.biochem.6b00889

42. Gulick AM, Starai VJ, Horswill AR, Homick KM, Escalante-semerena JC. The 1 . 75 Å crystal structure of acetyl-CoA synthetase bound to adenosine-5 ′ -propylphosphate and Coenzyme A. Biochemistry. 2003;42: 2866–2873. doi:10.1021/bi0271603

43. Shah MB, Ingram-smith C, Cooper LL, Qu J, Meng Y, Kerry S, et al. The 2.1Å crystal structure of an acyl-CoA Synthetase from *Methanosarcina acetivorans* reveals an alternate acyl binding pocket for small branched acyl substrates. Proteins. 2009;77: 685–698. doi:10.1002/prot.22482.

44. Sundlov J a., Fontaine DM, Southworth TL, Branchini BR, Gulick AM. Crystal structure of firefly luciferase in a second catalytic conformation supports a domain alternation mechanism. Biochemistry. 2012;51: 6493–6495. doi:10.1021/bi300934s

45. Reger AS, Carney JM, Gulick AM. Biochemical and crystallographic analysis of substrate binding and conformational changes in acetyl-CoA synthetase. Biochemistry. 2007;46: 6536–6546. doi:10.1021/bi6026506

46. Saraste M, Sibbald PR, Wittinghofer A. The P-loop — a common motif in ATP- and GTP-binding proteins. Trends Biochem Sci. 1990;15: 430–434. doi:10.1016/0968-0004(90)90281-F

47. May JJ, Kessler N, Marahiel MA, Stubbs MT. Crystal structure of DhbE, an archetype for aryl acid activating domains of modular nonribosomal peptide synthetases. Proc Natl Acad Sci. 2002;99: 12120–12125. doi:10.1073/pnas.182156699

48. Conti E, Stachelhaus T, Marahiel MA, Brick P. Structural basis for the activation of phenylalanine in the non-ribosomal biosynthesis of gramicidin S. EMBO J. 1997;16: 4174–4183. doi:10.1093/emboj/16.14.4174

49. Lu X, Rong Z, Indrajeet S, Li X, Kumar G, Swaminathan S, et al. Stable analogues of OSB-AMP: potent inhibitors of MenE, the O- succinylbenzoate-CoA synthetase from bacterial menaquinone biosynthesis. Chembiochem. 2012;13: 129–136. doi:10.1002/cbic.201100585

50. Chang KH, Xiang H, Dunaway-Mariano D. Acyl-adenylate motif of the acyl-adenylate/thioester-forming enzyme superfamily: a site-directed mutagenesis study with the *Pseudomonas sp.* Strain CBS3 4-chlorobenzoate:coenzyme A ligase. Biochemistry. 1997;36: 15650–15659. doi:10.1021/bi971262p

51. Stuible H-P, Büttner D, Ehlting J, Hahlbrock K, Kombrink E. Mutational analysis of 4-coumarate: CoA ligase identifies functionally important amino acids and verifies its close relationship to oher adenylate-forming enzymes. FEBS Lett. 2000;467: 117–122. doi:10.1016/S0014-5793(00)01133-9

52. Starai VJ, Escalante-Semerena JC. Identification of the protein acetyltransferase (Pat) enzyme that acetylates acetyl-CoA synthetase in *Salmonella enterica*. J Mol Biol. 2004;340: 1005–1012. doi:10.1016/j.jmb.2004.05.010

53. Hallows WC, Lee S, Denu JM. Sirtuins deacetylate and activate mammalian acetyl-CoA synthetases. Proc Natl Acad Sci. 2006;103: 10230–10235. doi:10.1073/pnas.0604392103

54. Renilla S, Bernal V, Fuhrer T, Castaño-Cerezo S, Pastor JM, Iborra JL, et al. Acetate scavenging activity in *Escherichia coli*: interplay of acetyl–CoA synthetase and the PEP–glyoxylate cycle in chemostat cultures. Appl Microbiol Biotechnol. 2012;93: 2109–2124. doi:10.1007/s00253-011-3536-4

55. Castaño-Cerezo S, Bernal V, Post H, Fuhrer T, Cappadona S, Sánchez-Díaz NC, et al. Protein acetylation affects acetate metabolism, motility and acid stress response in *Escherichia coli*. Mol Syst Biol. 2014;10: 1–16. doi:10.15252/msb.20145227

56. Zhang J, Sprung R, Pei J, Tan X, Kim S, Zhu H, et al. Lysine acetylation is a highly abundant and evolutionarily conserved modification in *Escherichia coli*. Mol Cell Proteomics. 2009;8: 215–225. doi:10.1074/mcp.M800187-MCP200

57. Kuhn ML, Zemaitaitis B, Hu LI, Sahu A, Sorensen D, Minasov G, et al. Structural, kinetic and proteomic characterization of acetyl phosphate-dependent bacterial protein acetylation. PLoS One. 2014;9: e94816. doi:10.1371/journal.pone.0094816

58. Baeza J, Dowell JA, Smallegan MJ, Fan J, Amador-Noguez D, Khan Z, et al. Stoichiometry of site-specific lysine acetylation in an entire proteome. J Biol Chem. 2014;289: 21326–21338. doi:10.1074/jbc.M114.581843

59. Schilling B, Christensen D, Davis R, Sahu AK, Hu LI, Walker-Peddakotla A, et al. Protein acetylation dynamics in response to carbon overflow in *Escherichia coli*. Mol Microbiol. 2015;98: 847–863. doi:10.1111/mmi.13161

60. De Diego Puente T, Gallego-Jara J, Castaño-Cerezo S, Sánchez VB, Espín VF, De La Torre JG, et al. The protein acetyltransferase PatZ from *Escherichia coli* is regulated by autoacetylation-induced oligomerization. J Biol Chem. 2015;290: 23077–23093. doi:10.1074/jbc.M115.649806

61. Mitchell C, Tucker AC, Escalante-Semerena JC, Gulick AM. The Structure of *S. lividans* acetoacetyl-CoA synthetase shows a novel interaction between the C-terminal extension and the N- terminal domain. Proteins. 2015;83: 575–581. doi:10.1002/prot.24738.

62. Notley-mcrobb L, Death A, Ferenci T. The relationship between external glucose concentration and cAMP levels inside. Biochem J. 2006;143: 1909–1918. doi:10.1099/00221287-143-6-1909

63. Makman RS, Sutherland EW. Adenosine 3', 5´-Phosphate in *Escherichia coli*. J Biol Chem. 1965;240: 1309–1314.

Supplementary material

Table S1. Strains, plasmids and primers used in this study. Restriction nuclease sites are in grey. Bold typeface indicates the modified codon during site-directed-mutagenesis.

***E. coli* strain**	**Genotype**	**Source**
BL21 (DE3)	F– ompT gal dcm lon hsdSB(rB- mB-) λ(DE3)	Agilent Technologies
DH10B	F- mcrA Δ(mrr-hsdRMS-mcrBC) Φ80dlacZΔM15 ΔlacX74 endA1 recA1 deoR Δ(ara,leu)7697 araD139 galU galK nupG rpsL λ-	Invitrogen
Plasmid	**Genotype**	**Source**
ASKA*acs*	N-terminal, His6-tag overexpression vector, Cam^R. Encodes *acs* wt	ASKA collection [27]
pBAD24-*cobB*MBP	C-terminal, His6-tag-MBP overexpression vector, Kan^R. Encodes *cobB* wt.	[28]
ASKA*acs*^{T264A}	N-terminal, His6-tag overexpression vector, Cam^R. Encodes *acs* T264A	This study
ASKA*acs*^{K270A}	N-terminal, His6-tag overexpression vector, CamR. Encodes *acs* K270A	This study
ASKA*acs*^{D500A}	N-terminal, His6-tag overexpression vector, CamR. Encodes *acs* D500A	This study

ASKA*acs*^{K609A}	N-terminal, His6-tag overexpression vector, CamR. Encodes *acs* K609A	This study
pRSF*acs*^{k609ac}	Coexpression vector, Kan^{R}. Encodes His6-*acs*K609AMBERcodon/acetyl-lysyl-tRNA-synthetase AcKRS3/M*b*tRNA$_{CUA}$	This study
Primer	**Sequence**	
ASKA*acs*^{T264A} Fwd	CTGTTTATTCTCTA**CGC**CTCCGGTTCTACC	
ASKA*acs*^{T264A} Rev	GGTAGAACCGGAG**GCG**TAGAGAATAAACAG	
ASKA*acs*^{K270A} Fwd	CCGGTTCTACCGGT**GCA**CCAAAAGGTGTGCTG	
ASKA*acs*^{K270A} Rev	CAGCACACCTTTTGG**TGC**ACCGGTAGAACCGG	
ASKA*acs*^{D500A} Fwd	GTATTTCAG**CGG**CGCCGGCGCGCGTCGC	
ASKA*acs*^{D500A} Rev	GCGACGCGCGCC**GGC**GCCGCTGAAATAC	
ASKA*acs*^{K609A} Fwd	CTAAAACCCGCTCCG**GCG**CAATTATGCGCCGTATTC	
ASKA*acs*^{K609A} Rev	GAATACGGCGCATAATTG**CGC**CGGAGCGGGTTTTAG	
ASKA*acs*^{K609amber} Fwd	CTAAAACCCGCTCCGGC**TAG**ATTATGCGCCGTATTC	
ASKA*acs*^{K609amber} Rev	GAATACGGCGCATAAT**CTA**GCCGGAGCGGGTTTTAG	
pRSF*acs*^{k609ac} Fwd	GGTGGTGAATTCATGAGCCAAATTCACAAACACA	
pRSF*acs*^{k609ac} Rev	GGTGGTGGTACCTTACGATGGCATCGCGATAG	

Table S2. Quality parameters of the predicted Acs models constructed using Swiss-Model software.

Template (PDB code)	Seq. Identity (%)	QMEAN z-score	GMQE	Coverage
5c5e	25.14	-2.45	0.56	68-620
1ry2	48.34	-2.55	0.75	22 - 643
5bsm	22.73	-2.71	0.53	74-621
4fut	22.42	-3.38	0.5	78-621
5n9x	23.8	-3.7	0.5	78-621
5d6j	17.72	-3.8	0.49	78-622
5bur	23.99	-4.22	0.49	78-616
2y27	22.05	-4.81	0.33	253-614
3fcc	18.16	-5.3	0.48	79-619
5elo	30.75	-8.79	0.47	24-494

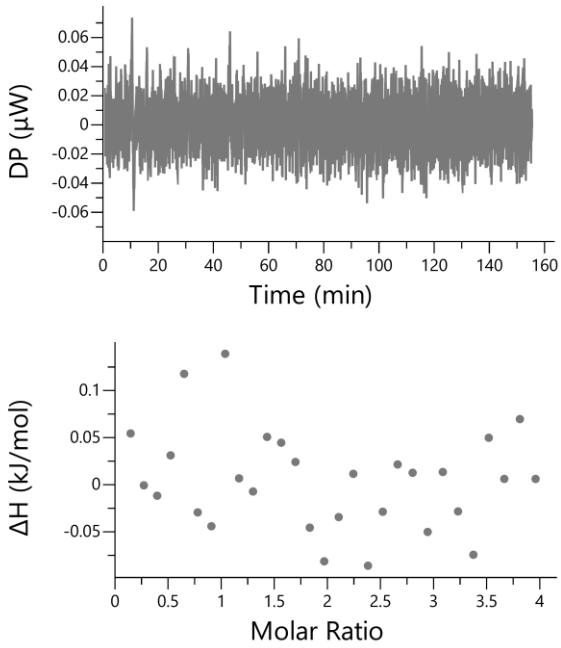

Figure S1. Acetate-binding to Acs protein followed using ITC. Raw data representing heat flow over time are reported (top panel) together with integrated head data after subtraction of the heat of dilution (bottom panel). The solid line represents the best-fit of the data, using a one-set-of-sites binding model.